Multistatic SAR Algorithm with Image Combination

Tommy Teer and Nathan A. Goodman
Department of Electrical and Computer Engineering, The University of Arizona
1230 E. Speedway Blvd., Tucson, AZ 85721-0104
Phone: 520-621-4462; Fax: 520-626-3144; goodman@ece.arizona.edu

Abstract— **This paper presents a flexible spotlight synthetic aperture radar (SAR) image formation algorithm that can be applied to multistatic configurations allowing the formation and combination of images from multiple passive receivers. Multiple receivers collecting radar returns at different angles can provide better detection against reduced radar cross section (RCS) objects and objects able to spread energy in many directions. A specialized time-frequency algorithm with selective matched filtering was developed for the monostatic case and extended to multiple passive receiver (multistatic) scenarios. The algorithm meets stringent geometric fidelity requirements necessary for combining images from multiple platforms imaging the scene and is shown to produce good results for both side-looking (broadside) and forward-looking (squinted) spotlight geometries. Simulations were used to test and validate the algorithms against both point reflectors and a simulated realistic scene for varying platform geometry/trajectory combinations.**

I. INTRODUCTION

A primary advantage of bistatic (or more generally, multistatic) radar over monostatic radar is the ability to collect radar returns reflected from a scene at angles different than that of the transmitted pulse. This is of special interest to military applications where targets can be specifically designed to reflect the transmitted energy in many directions, thereby minimizing the energy that is reflected back to the transmitter. In this paper, we consider multistatic imaging for the case where there is a single transmitter and multiple passive receivers on spatially separated platforms. A monostatic collection could coexist with the multistatic collection environment for the case when the transmitter also has a co-located receiver.

Multiple receivers enable sampling of the scene reflections from many different angles. Therefore, an object that scatters incident energy in many directions has a better chance of being detected when multiple receivers are present. Additionally, by combining images from multiple receivers, a composite view of the scene can be formed by incorporating energy received by all receivers. There are several possible benefits of combining images. The increase in signal-to-noise ratio (SNR) could result in a low-RCS target being detected in the composite image while not being detected in the image of any single-receiver image. Similarly, different components of a target may only scatter energy in a limited range of directions. Images from individual receivers may show returns from different components of a target; therefore, combining images could fill in components of a target allowing it to be successfully identified whereas any single receiver image may not provide enough information. Passive receivers are also less likely to be detected at short standoff ranges while the transmitter can remain at a safe standoff range.

As a result of its added complexity and narrow audience, Bistatic SAR (BSAR) imaging [3-7] has received much less attention than its monostatic counterpart. An overview of BSAR, addressing both imaging algorithms and practical hardware considerations such as coherency, is considered in [4] and a more rigorous coherency analysis is done in [8]. The polar-format algorithm (PFA) and range-migration algorithm (RMA) [2] used in monostatic collections are loosely extended to the BSAR case in [4-5]. A more in-depth study is given in [3] for extending the PFA to BSAR incorporating additional benefits. Although sparking significant advancement in this topic, neither multiple, passive platforms nor image combination are discussed.

In this paper, a time-frequency algorithm for multistatic SAR imaging is developed. The algorithm uses sub-intervals (which we call snapshots) of the SAR data collection record similar to that in [1], which allows multiple coarse-Doppler-resolution snapshots to be formed over the full collection interval. The range/Doppler coordinates of a reference snapshot are converted to inertial coordinates in the ground imaging and focus plane. Then, phase corrections are applied to the remaining snapshots in order to align and linearize the phase of the inertial locations across snapshots before the final fine-resolution image is formed. This is done for both the monostatic and multistatic platforms. The fine-resolution range/Doppler images of all receivers are then placed into a common image display plane allowing their combination into a composite image.

In the scenarios simulated for this paper, the transmitting platform flies along a path while radiating a desired ground area. The passive receiver-only platforms are flying along other paths collecting reflections from the scene. The coherent reference point (CRP) for all receivers is the same, but as a result of orientation/geometry differences, the available imaging area between receivers will not be the same. A portion of the area contained in an image from one receiver may not be in another as a result of differences in the bistatic two-way antenna pattern.

In these scenarios, the transmitting platform will also contain a receiver taking a monostatic collection of the scene while the individual receivers in the multistatic configuration are also forming images. Having a monostatic image

0-7803-9497-6/06/$20.00 © 2006 IEEE.

provides an excellent reference image and has potential advantages for reconciling images and removing phase errors in the multistatic receivers when practical considerations such as navigation and hardware errors are introduced.

II. ALGORITHM

A coherent train of chirp pulses is transmitted, which illuminates the scene for all receivers. The parameters of the transmitted waveform are selected to accommodate the requirements of all receivers. For example, the pulse repetition frequency (PRF) is selected to allow all receivers (including the monostatic) to receive the signal from their entire respective range swath before the next pulse is transmitted. Stretch processing is used in each receiver.

The first step in the algorithm is to motion compensate the data to a common inertial point for all receivers. This provides a common central location and maximizes the amount of overlap in receiver coverage areas. Then, each receiver calculates its own set of parameters needed for the snapshot-based method. For example, each receiver calculates its own snapshot, or sub-interval, duration which is short enough to prevent a location from migrating through a range/Doppler cell during the sub-interval, but long enough to get sufficient resolution. As mentioned in [1], overlapping of the snapshots is necessary to control sidelobes. Next, a reference snapshot is chosen. This is usually the snapshot nearest the center of the full processing interval. The inertial locations corresponding to the center of every range/Doppler cell is determined for the reference snapshot. Since the time interval of each snapshot is shorter than the full processing interval, each snapshot provides a low-resolution Doppler image corresponding to different sub-intervals of the collection time.

As the platforms move, the inertial points calculated from the reference snapshot will migrate through range and Doppler over the remaining snapshots. Moreover, the same inertial point will migrate differently for each receiver. Our algorithm forces the inertial coordinates calculated from the reference snapshot back into their reference range/Doppler bins for all snapshots. This is accomplished by applying deterministic phase corrections and integer range bin shifts. However, since the inertial points used to track and compensate for range-Doppler migration were identified from the range-Doppler bins of a coarse-resolution snapshot, only this finite set of inertial locations are perfectly corrected. This implies that once the final fine-resolution image is formed, some of the pixels will be perfectly match filtered while the remaining locations receive favorable corrections.

The next step in the algorithm is to combine the snapshots to form a high-resolution image for each receiver. This is accomplished via the chirp-z transform since only a fraction of the Doppler bandwidth needs to be computed in order to extract multiple high-resolution cells from a given coarse-resolution cell formed earlier in the process. Fig. 1 highlights the processing chain after the initial motion compensation.

In the proposed algorithm, it is important to be able to accurately map range/Doppler bins to inertial ground-plane locations and vice versa. Obviously, these mappings are much more difficult for each of the bistatic platforms than for the monostatic platform. Given the North-East-Down (NED) position (P_x, P_y, P_z) of a platform with respect to the CRP, NED velocity of the platform, (V_x, V_y, V_z), the North inertial position of a stationary reflector with range, r, and range-rate, $\dot{r}$, is

$$N = -\frac{\left(\begin{array}{l} -V_x P_x - V_y P_y + \frac{V_y}{2\left((V_y)^2 + (V_x)^2\right)} \cdot \\ \left[\begin{array}{l} -2r\dot{r}V_y + 2(V_x)^2 P_y + 2(V_y)^2 P_y + 2(V_z) P_z V_y \\ \pm 2\sqrt{-(V_x)^2 (P_z)^2 (V_z)^2 - (V_y)^2 (P_z)^2 (V_x)^2 - (V_x)^4 (P_z)^2} \\ +2(V_x)^2 P_z V_z r\dot{r} - (V_x)^2 \dot{r}^2 r^2 + (V_x)^4 r^2 + (V_y)^2 r^2 (V_x)^2 \end{array} \right] \\ -P_z V_z + r\dot{r} \end{array} \right)}{V_x}$$

and the East inertial position is

$$E = \frac{1}{2\left((V_y)^2 + (V_x)^2\right)} \cdot \left[\begin{array}{l} -2r\dot{r}V_y + 2(V_x)^2 P_y + 2(V_y)^2 P_y + 2(V_z) P_z V_y \\ \pm 2\sqrt{-(V_x)^2 (P_z)^2 (V_z)^2 - (V_y)^2 (P_z)^2 (V_x)^2 - (V_x)^4 (P_z)^2} \\ +2(V_x)^2 P_z V_z r\dot{r} - (V_x)^2 \dot{r}^2 r^2 + (V_x)^4 r^2 + (V_y)^2 r^2 (V_x)^2 \end{array} \right],$$

which were found by mapping inertial positions into range and range-rate, setting the z-location of the inertial point to zero (assumes a flat ground plane), and solving the simultaneous equations for the North and East positions. Under bistatic conditions, mapping inertial locations into bistatic range and range-rate is accomplished by finding the range and range-rate to the location with respect to the two individual platforms and taking the average. Unfortunately, mapping a range/range-rate coordinate pair back to an inertial location is not as straightforward under bistatic conditions. An attempt was made using a commercial math package to solve the simultaneous bistatic equations. When both inertial coordinates were unknown, the tool was unsuccessful in determining a solution, but when one of the coordinates was known, a solution was obtained.

Since mapping from inertial coordinates to range/range-rate pairs was feasible, range/range-rate coordinates were calculated for a large set of inertial locations within the scene of interest. These coordinates were subsequently used to interpolate one of the inertial coordinates. This coordinate could then be used to calculate the other. Fortunately, the mapping from range/range-rate to inertial coordinates only needs to be done for the reference snapshot, so this step adds little computational burden overall.

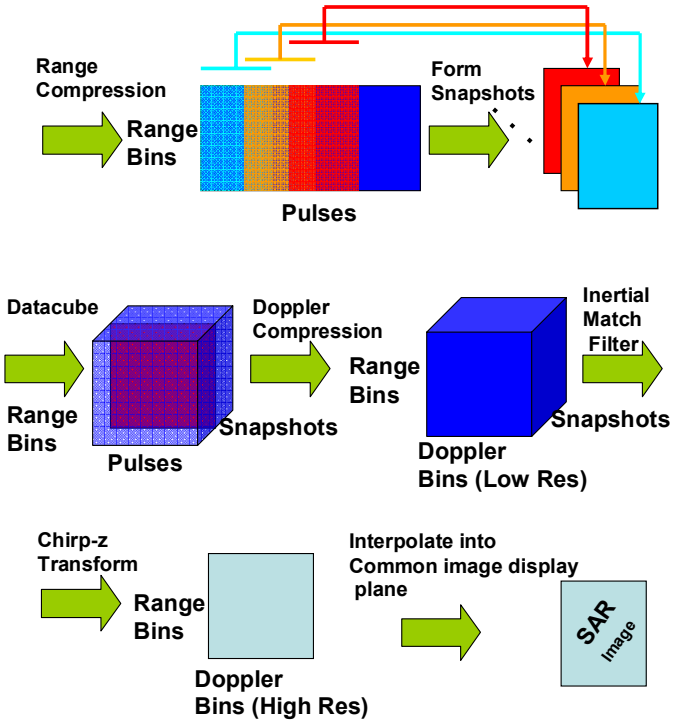

Figure 1. Processing Chain

III. RESULTS

In this section, we present results obtained via a high-fidelity radar data simulator. We consider several scenarios with different look geometries and bistatic configurations. We first perform simulations where the scene contains a few, sparsely located point scatterers. Then we consider a more realistic scene with targets and distributed clutter.

The first example consists of a transmitter/receiver platform at broadside geometry located at a range of 10 km while two passive receivers are flying parallel to the transmitter at a range of 3 km with 10-degree bistatic angles as shown in Fig. 2. The images from the 3 receivers are shown in a common image display plane in Fig 3. The phase history of the lower left point reflector in receiver #2 before and after correction is shown in Fig. 4. The nonlinear portion of the phase is nearly zero after correction. Fig. 5 shows the non-coherent combination of the images created by summing the power in each image pixel by pixel. No image manipulation was required.

A second example scenario is depicted in Fig. 6. In this example the transmitter/receiver platform is observing the scene at 60 degrees off broadside while the two passive receivers are traveling as shown. The three resulting receiver images are shown in Fig. 7. Overlaying the images are markers indicating the inertial locations used for match filtering in each of the respective receivers showing how the points differ between receivers. The phase history of a point reflector in receiver #2 is shown in Fig. 8. The dominantly quadratic phase is much larger for this geometry, and even though the algorithm has significantly reduced the nonlinear portion, a small quadratic remains. Sidelobe levels have also increased slightly on some of the points and can be seen in the combined image in Fig. 9. Note that Hamming windows were used throughout for sidelobe suppression so the 50 dB dynamic range in the image is sufficient to reveal any artifacts.

To provide a better perspective on these results a distributed clutter scene was simulated. The scene consists of two helicopters (lower left and upper right) and an A-10 (near center). Two roads lined with small trees separated by a median run through the image at an elevation several meters lower than the ground on which the aircraft are parked. The geometry is similar to the first example, but the scene is 15 degrees off broadside from the transmitting platform and the bistatic angles are 15 degrees. The A-10 is difficult to pick out in each individual receiver image as seen in Fig. 10, but is more clear in the combined image in Fig. 11.

IV. ALGORITHM LIMITATIONS

Although the algorithm has proven to be robust, it does have limitations and tradeoffs to consider. When moving away from the reference snapshot where the inertial locations used to match filter were determined, an attempt is made to force those particular locations back to the center of the same cell and make its phase zero. When an inertial location migrates into another range cell, all range cells in that Doppler bin in that snapshot can be shifted the same amount since they moved in range according to their current range-rate (in a bistatic sense) which is measured by the Doppler cell they are currently located in. Unlike range, when a inertial location migrates into other Doppler cells, the Doppler cells for that range bin cannot be shifted since range-acceleration determines this migration and, unfortunately, is not a function of range bin alone. Hence, the algorithm cannot readily compensate for locations with large range-accelerations.

The first reaction to counteract this deficiency would be to make the individual snapshot durations smaller which would, in turn, increase the bandwidth of the Doppler cells giving locations more "room" to accelerate before crossing into neighboring cells. However, this also reduces the number of points being matched filtered resulting in larger spatial extents between matched filtered locations (e.g. the markers across the images in Fig. 7 would have further separation). This is one of many trades that can be made.

Additionally, inertial points contained in a range/Doppler cell, but not at the center of the cell may be associated with more than one match filter location over the collection interval (i.e. it gets the correction for one location and then another). This results in small phase discontinuities at these transition boundaries raising the sidelobe levels.

Finally, these limitations coupled with each receiver having a different set of inertial matched filter locations

makes coherent combination of the images difficult. The only common point in all the images that is guaranteed to have known phase is the CRP. Determining the phase in each pixel of each receiver image is a formidable task.

V. Practical Considerations

A practical scenario would involve a high power transmitter flying at a safe standoff range while passive, preferably unmanned, platforms (UAVs, missiles) fly closer to the scene. The passive receivers communicate with the transmitter via a low bandwidth communication link for sending their navigation data. The transmitter decides which passive receivers have trajectories consistent and meaningful for forming bistatic images, and sends the receivers the transmit waveform parameters such as PRF, chirp rate, pulse-width, time of first transmit, and its own navigation updates, for example. The receivers collect and process the data forming bistatic images, sending the images back to the transmitter. The transmitter concurrently forms a monostatic image of the scene making an assessment of the scene using the monostatic and multiple bistatic images. With ideal navigation data and hardware coherency the images can be combined as previously shown. However, navigation errors will result in spatially variant geometric distortion in each image presenting problems for image combination. Feature registration between the monostatic image and each passive image could mitigate these effects by removing the spatially variant geometric distortion unique to each receiver before combination

VI. Conclusion

This paper presented a flexible multistatic SAR image formation algorithm predicated on mapping bistatic range/Doppler pairs into inertial coordinates and vice-versa. Simulation results for both simulated point source scenes and a simulated distributed clutter scene under various geometries were offered. Although mapping range/Doppler coordinates under bistatic conditions to inertial locations (in the ground plane) could not be evaluated with a closed form expression, results from mapping inertial locations into range/Doppler coordinates under the same bistatic condition were used to interpolate the range/Doppler to inertial mapping. With proper parameter selection and additional work to mitigate real-world affects, the algorithm can be both efficient and practical.

References

[1] Doerry, A.W., "Synthetic aperture radar processing with polar formatted subapertures", Sandia National Laboratories, IEEE, 1995.

[2] Carrara, W.G., R.S. Goodman, R.M. Majewski, Spotlight Synthetic Aperture Radar, Norwood, MA, Artech House, 1995.

[3] Rigling, B. D., and Moses, R., "Polar format algorithm for bistatic SAR", IEEE Transactions on Aerospace and Electronic Systems, Oct. 2004, pp. 1147–1159.

[4] Horne, A. M., and Yates, G, "Bistatic synthetic aperture radar", IEE Radar 2002, Oct. 2002, pp. 6–10.

[5] Lowe, M. , "Algorithms for high resolution bistatic SAR", IEE Radar 2002, Oct. 2002, pp. 512–515.

[6] Arikan, O., and Munson, D. C., "A tomographic formulation of bistatic synthetic aperture radar", In Proceedings of ComCon '88, Oct. 1988, p. 418.

[7] Soumekh, M., "Bistatic synthetic aperture radar inversion with application in dynamic object imaging", IEEE Transactions on Signal Processing, 39 , Sept. 1991, pp. 2044–2055.

[8] Weiß, M. , "Synchronisation of Bistatic Radar Systems", IEEE, 2004, pp. 1750-1754.

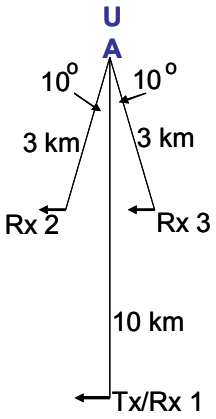

Figure 2. Broadside Example Geometry

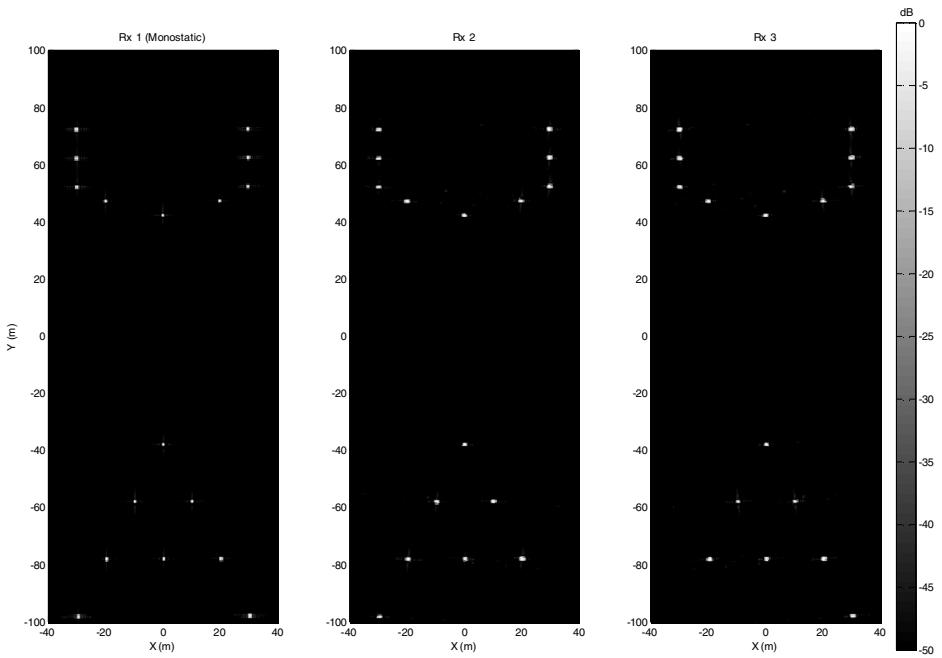

Figure 3. Receiver Images from First Example

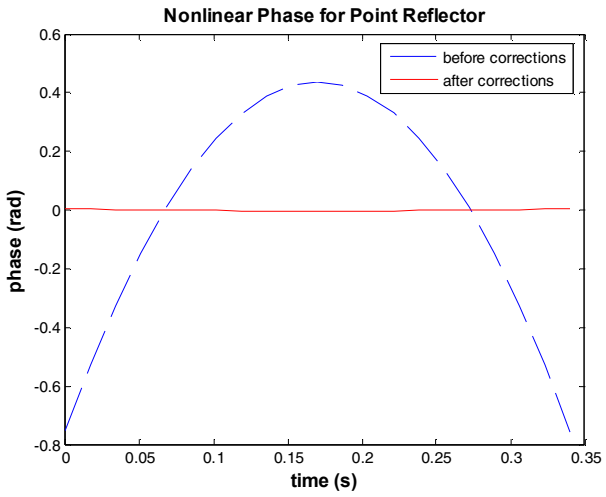

Figure 4. Nonlinear Phase Components Before and After Correction

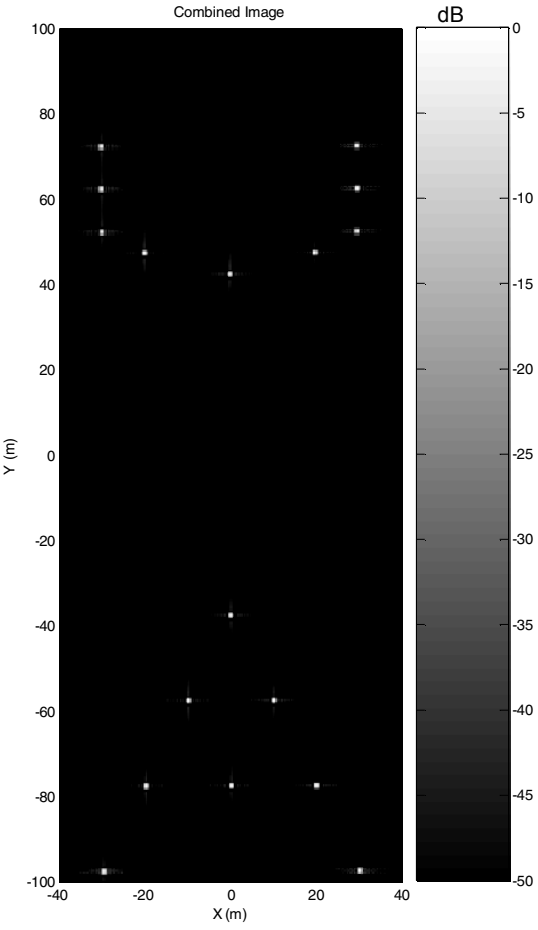

Figure 5. Combined Image from First Example

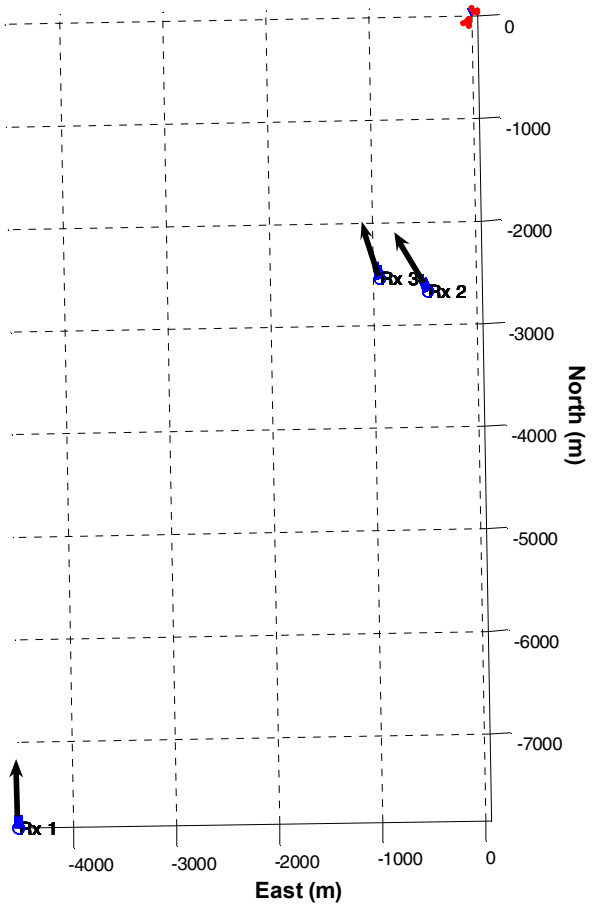

Figure 6. Squinted Example Geometry

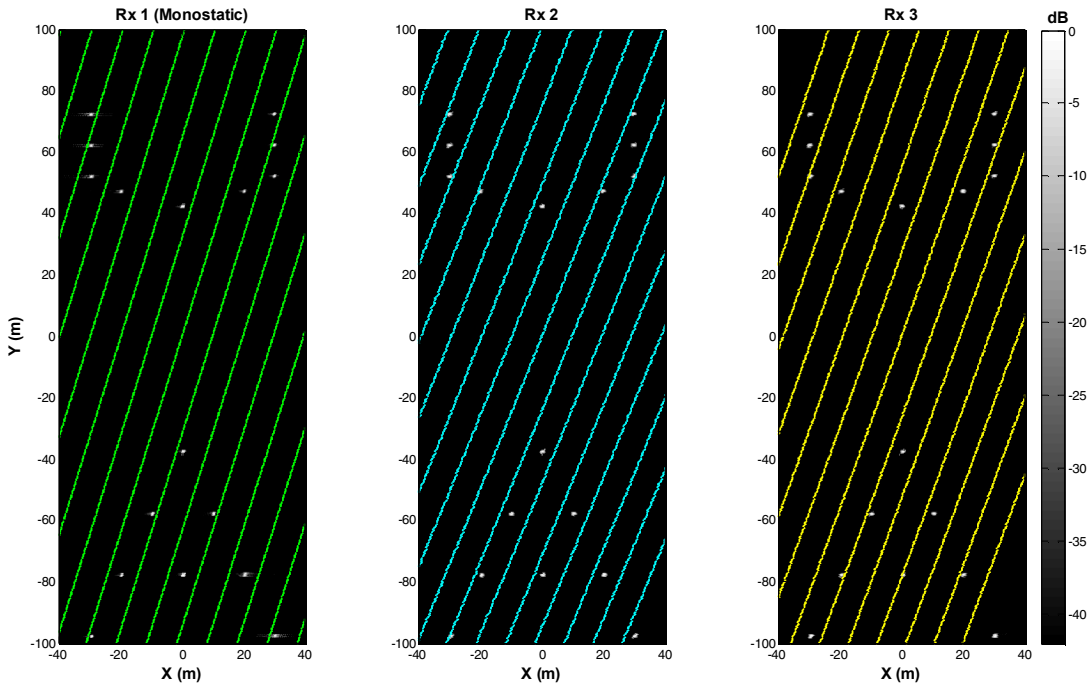

Figure 7. Receiver Images from Second Example

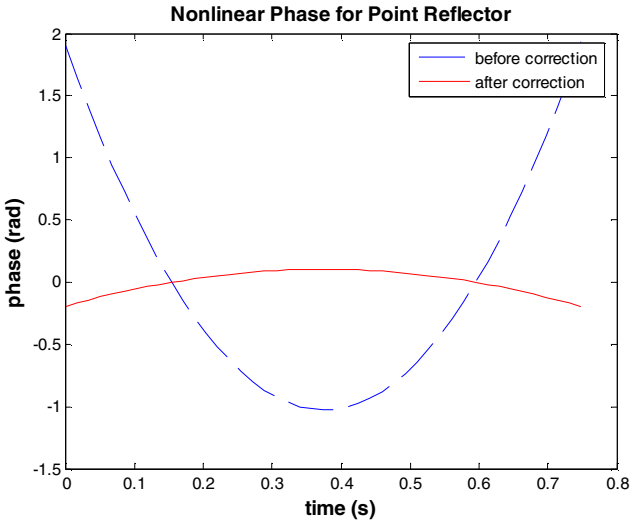

Figure 8. Nonlinear Phase from Second Example

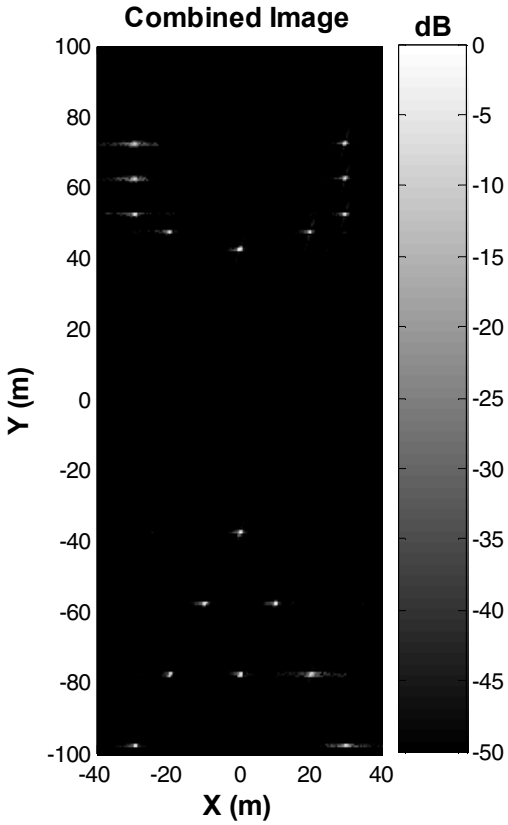

Figure 9. Combined Image from Second Example

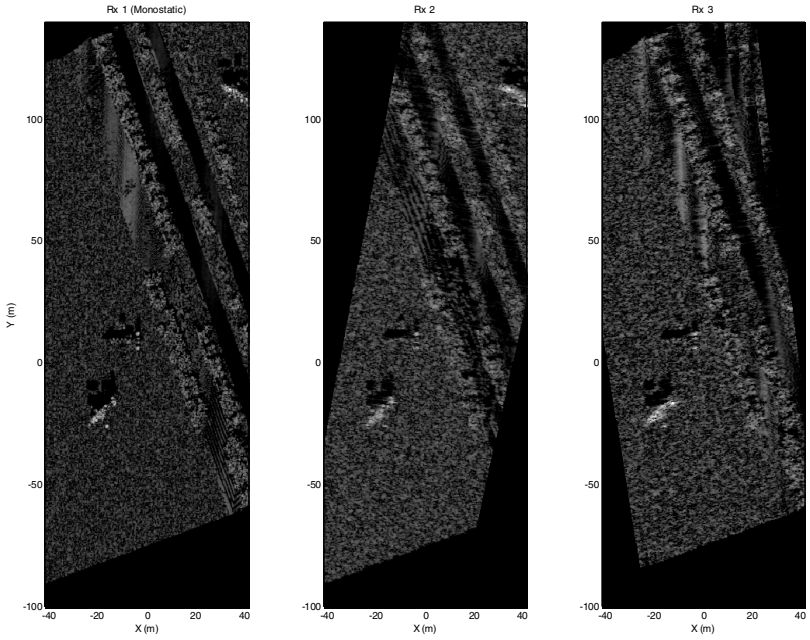

Figure 10. Receiver Images from Distributed Clutter Example

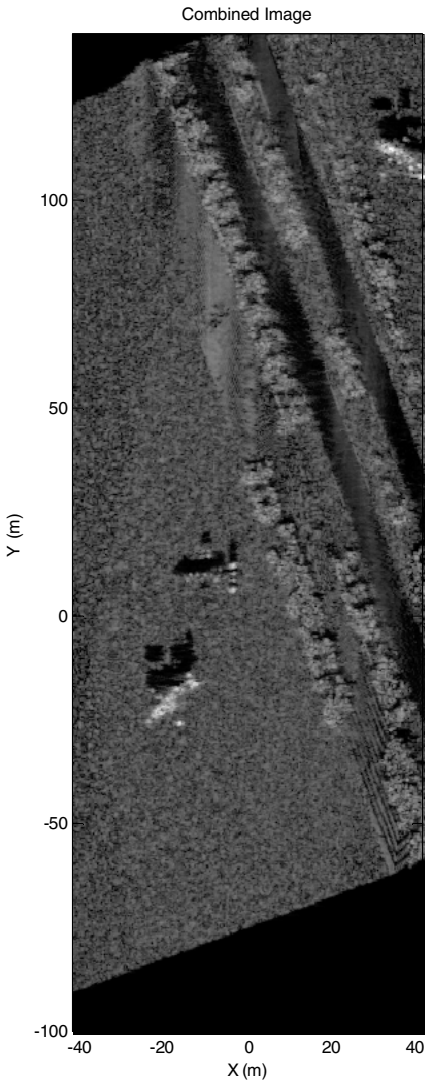

Figure 11. Combined Image from Distributed Clutter Example